

BOUNDARY HOMOGENIZATION FOR PERIODIC ARRAYS OF ABSORBERS*

CYRILL B. MURATOV[†] AND STANISLAV Y. SHVARTSMAN[‡]

Abstract. We introduce a homogenization procedure for reaction-diffusion equations in domains whose boundary consists of small alternating regions with prescribed Dirichlet and Neumann data of comparable areas. The homogenized problem is shown to satisfy an effective Dirichlet boundary condition which depends on the geometry of the small-scale boundary structure. This problem is also related to finding the effective trapping rate for a Brownian particle next to a surface with a periodic array of perfect absorbers. We use the method of optimal geometric grids to numerically solve the unit cell problem of homogenization. The geometric homogenization factor is obtained for a number of cell geometries (stripes, square and hexagonal arrays of disk-shaped absorbers or emitters) as a function of the surface area fraction occupied by the absorbers. Empirical analytical expressions that give excellent fits to data for the entire range of area fractions and correct asymptotic behaviors in the limits of small and large absorber area fractions are proposed.

Key words. reaction-diffusion systems, Brownian motion, heterogeneous boundaries, homogenization

AMS subject classifications. 35B27, 35K57, 65N02, 65N35

DOI. 10.1137/070692832

1. Introduction. Consider a Brownian particle released from a heterogeneous boundary composed of perfectly absorbing patches on an otherwise reflecting surface. Depending on the particular application, one might be interested in the flux of particles from a patchy surface, in the statistical properties of trajectories leading to capture, or in the rate of a chemical reaction if the particle enters a reacting medium [2, 16, 24, 28, 36, 43]. Such problems are interesting for several reasons. First, patterned surfaces can be robustly manufactured using modern microfabrication techniques and find applications in catalysis and electrochemistry [16]. Second, strongly heterogeneous boundary value problems of reaction-diffusion type arise in modeling a variety of nonlinear phenomena, in particular, problems of cell signaling in developmental biology [2, 24, 31, 40]. In addition, these problems share certain mathematical aspects with problems arising in a number of other fields, notably in electrostatics [18, 21, 22, 23].

The interest in problems with patchy surfaces goes back to the 1930's in connection with the design of vacuum tubes (see [18, 23] and the references therein). Already in these early studies it was realized that when the sizes of individual patches are much smaller than the physical length scale of the problem, such problems can be efficiently treated by a homogenization approach in which the mixed Dirichlet–Neumann boundary condition on a patchy surface is replaced by an effective *homogeneous* boundary condition. These ideas have been further developed in the mathematical works of many authors (see, e.g., [8, 9, 20, 21, 22, 25, 34]).

*Received by the editors May 23, 2007; accepted for publication (in revised form) September 19, 2007; published electronically April 11, 2008. This work was supported by the NIH through grant R01 GM076690.

<http://www.siam.org/journals/mms/7-1/69283.html>

[†]Department of Mathematical Sciences, New Jersey Institute of Technology, Newark, NJ 07102 (muratov@njit.edu).

[‡]Department of Chemical Engineering and Lewis Sigler Institute for Integrative Genomics, Princeton University, Princeton, NJ 08544 (stas@princeton.edu).

More recently, the interest in problems with fine-grained heterogeneous boundary conditions has been renewed in connection with the studies of cell communication by diffusing signals [2, 24, 40]. To give an illustrative example, consider a monolayer of cells covered by a thick layer of extracellular medium. In the extracellular medium, a signaling molecule can diffuse with diffusion coefficient D_s or be converted to an inactive form via an enzymatic reaction. Assuming Michaelis–Menten kinetics, we can write the equation for the concentration $S = S(x, y, z, t)$ of the signal in the extracellular medium occupying the region $z > 0$ as

$$(1.1) \quad S_t = D_s \Delta S - \frac{V_m S}{K_m + S},$$

where Δ is the three-dimensional Laplacian and V_m, K_m are Michaelis–Menten constants. The signaling molecules, in turn, are secreted by the cells at the bottom of the extracellular medium (assumed to be at $z = 0$). This problem becomes strongly heterogeneous if the cells in the layer consist of groups with different levels of gene expression, in particular, when a cell surface receptor to which the signaling molecule can bind is expressed at different levels in different cells or patches of cells. Examples of this situation abound both in the *in vivo* epithelial layers and in cell tissue cultures [3, 41].

For simplicity, let us assume that the layer consists of only two distinct groups of cells, with the majority not expressing the receptor and the minority expressing it at sufficiently high levels. The minority cells are also assumed to be arranged periodically in the cell layer. In this situation the majority cells will be able to secrete the signal, while the minority cells will act as absorbers by the essentially irreversible binding of the signaling molecules to the cell surface receptors followed by endocytosis [2, 24, 40]. This leads to the following boundary condition on the surface of the cell layer:

$$(1.2) \quad -D_s S_z(x, y, 0, t)|_{\text{majority}} = Q_s g(x, y, t), \quad S(x, y, 0, t)|_{\text{minority}} = 0,$$

where Q_s is the maximum secretion rate and g is the normalized secretion rate at a given position on the cell layer at a given moment.

Under reasonable biophysical assumptions the size l of a single cell can be considerably smaller than the diffusion length $L = (D_s K_m / V_m)^{1/2}$ of the signal in the extracellular medium, justifying a continuum modeling approach [2, 24, 26, 40]. Since the seminal contribution by Berg and Purcell, problems with such fine-grained patchy surfaces have been treated within the effective medium approximation in which the heterogeneous surface is replaced by a homogeneous one, with a partially absorbing boundary condition uniform over the entire surface [4, 6, 35, 42]. The Berg–Purcell approximation is derived for the case of circular absorbers and asymptotically small absorber surface area fraction. Recently, we have developed a computational homogenization procedure for periodic and random dispersions of circular absorbers [4, 5]. This procedure was found to provide an excellent approximation for the statistics of Brownian particle motion for arbitrary absorber area fractions, is not limited to circular and perfectly absorbing absorbers, and can be extended to surfaces covered by the mixtures of absorbers of different sizes. Mathematically, however, this approach had been justified only for small absorber area fractions, thus essentially covering only the Berg–Purcell limit [9, 22, 25].

In this paper we clarify the nature of the approximation proposed by us in our earlier works [4, 5] by formulating a limit problem which gives rise to a homogenized boundary condition in the limit $\varepsilon = l/L \rightarrow 0$. Surprisingly, the homogenized boundary condition found in the limit problem turns out to be different from the mixed

boundary condition used in earlier studies, thus resulting in a new class of boundary homogenization problems. Nevertheless, as we show below, using the mixed boundary condition derived in [4, 5] is also consistent with the homogenization limit when $l \ll L$.

For surfaces covered by circular absorbers, we propose a functional form of the homogenized boundary condition that is valid over a wide range of absorber area fractions and can be used for both types of the considered two-dimensional absorber lattices. We find that while the value of the geometric factor in the homogenized boundary condition depends strongly on the surface area fraction occupied by the absorbers, it is practically independent of the lattice type (see also [12, 19]). In addition, we provide new asymptotic results on the behavior of the homogenized boundary condition at high absorber area fractions. For the case of striped surfaces, we rederive the effective boundary condition first obtained by Moizhes in [23].

Most of our numerical results are based on the novel algorithm for treating exterior boundary value problems [10, 11, 15]. In the next two sections, we formulate the homogenization procedure and outline the algorithm for solving the unit cell problem of homogenization. We then obtain accurate numerical data for the geometric homogenization factor for a range of cell geometries and analyze its asymptotic behaviors at small and large absorber area fractions. Guided by these asymptotic results, we propose analytical expressions for the geometric homogenization factor as a function of the absorber area fraction for the considered geometries, which provide excellent fits to data. In the end, we discuss possible extensions of our results.

2. Problem formulation. We start by considering a general initial-boundary value problem for a reaction-diffusion equation in the domain $\Omega \subset \mathbb{R}^3$ with smooth boundary. We are interested in the situation in which the boundary of Ω contains a series of alternating small-scale “absorbers” and “emitters,” i.e., regions with prescribed Dirichlet and Neumann data, respectively. Denoting the absorbing portion of $\partial\Omega$ by $\partial\Omega_0^\varepsilon$, where $\varepsilon \ll 1$ characterizes the length scale of the absorbers, we obtain

$$(2.1) \quad u_t^\varepsilon = \Delta u^\varepsilon + f_\varepsilon(\mathbf{x}, t, u^\varepsilon), \quad u^\varepsilon(\mathbf{x}, 0) = u_0^\varepsilon(\mathbf{x}),$$

$$(2.2) \quad u^\varepsilon|_{\partial\Omega_0^\varepsilon} = v_\varepsilon(\mathbf{x}, t), \quad \nu \cdot \nabla u^\varepsilon|_{\partial\Omega \setminus \partial\Omega_0^\varepsilon} = g_\varepsilon(\mathbf{x}, t).$$

Here $u^\varepsilon = u^\varepsilon(\mathbf{x}, t)$ is scalar, \mathbf{x} is the Cartesian coordinate of a point in Ω , and ν is the outward normal to $\partial\Omega$. A natural question which arises in relation with the initial-boundary value problem presented above is whether, perhaps after a suitable rescaling of $f_\varepsilon, v_\varepsilon, g_\varepsilon$, there is a limit problem associated with (2.1) and (2.2) for a family of $\partial\Omega_0^\varepsilon$ and $f_\varepsilon, v_\varepsilon, g_\varepsilon$ when $\varepsilon \rightarrow 0$ and what that limit problem actually is. In this paper we consider the particular scaling

$$(2.3) \quad f_\varepsilon = f, \quad u_0^\varepsilon = u_0, \quad v_\varepsilon = v, \quad g_\varepsilon = \varepsilon^{-1}g,$$

corresponding to the presence of *strong* boundary sources. This limit can be derived from the model of cell signaling considered in the introduction by assuming that $Q_s \sim D_s K_m / l$. Indeed, it is easy to see that (2.1)–(2.3) with $f = u/(1+u)$ and $v = 0$ can be obtained by rescaling $\mathbf{x} \rightarrow L\mathbf{x}$, $t \rightarrow (K_m/V_m)t$, setting $u = S/K_m$, and sending $\varepsilon = l/L \rightarrow 0$.

Mathematical studies of homogenization problems in the present context go a long way back to the works of Marchenko and Khruslov [20, 21, 22]. A related problem of the Neumann sieve has also been investigated by many authors [8, 9, 25, 34]. Let us also mention some recent related studies of nonlinear problems of reaction-diffusion

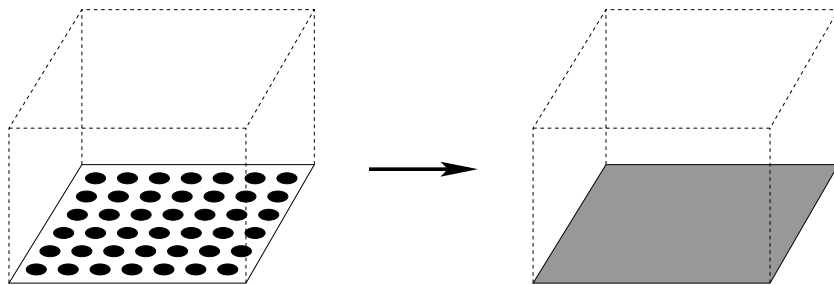


FIG. 2.1. *The schematics of the homogenization problem. The mixed Dirichlet (black) and Neumann (white) portions of the boundary of the original problem (left) are transformed into an effective inhomogeneous Dirichlet boundary condition (gray) in the homogenized problem (right).*

type [1, 14, 17, 22]. We would like to point out, however, that the problem we are considering here is unusual in a number of ways. In our formulation, we allow for a suitable rescaling of the Neumann data, which leads to a new type of homogenized boundary condition. Also, for this reason the dependence of the effective boundary condition on the geometry of the absorbing portion of the boundary remains non-trivial even when the absorbers and the emitters occupy comparable portions of the boundary and in general cannot be expressed in terms of the capacities of individual absorbers in free space (see also [4, 5]).

In this paper we will use formal asymptotic arguments to show that the limit problem associated with (2.1)–(2.3) is

$$(2.4) \quad u_t = \Delta u + f(\mathbf{x}, t, u), \quad u(\mathbf{x}, 0) = u_0(\mathbf{x}), \quad u|_{\partial\Omega} = v(\mathbf{x}, t) + \bar{\kappa}^{-1}(\mathbf{x})g(\mathbf{x}, t),$$

where u is the homogenization limit solution for u^ε as $\varepsilon \rightarrow 0$, and $\bar{\kappa}$ is a geometric factor depending on the shape of absorbers $\partial\Omega_0^\varepsilon$. The value of $\bar{\kappa}$ is also related to the effective trapping rate κ for the Brownian particles near the boundary $\partial\Omega$:

$$(2.5) \quad \kappa = \varepsilon^{-1}\bar{\kappa}.$$

In fact, in view of (2.5) the mixed boundary condition

$$(2.6) \quad \nu \cdot \nabla u_\varepsilon|_{\partial\Omega} = \kappa(v - u_\varepsilon) + \varepsilon^{-1}g$$

becomes indistinguishable from (2.4) in the limit $\varepsilon \rightarrow 0$. This justifies the use of (2.6) as a uniform approximation in [4, 5] that remains valid in the Berg–Purcell limit [6, 9, 20, 21, 22, 25] as well. We note that the idea of homogenizing the boundary condition on $\partial\Omega$ using a mixed boundary condition was first proposed in the studies of the screening effect of metallic grids on the electrostatic field in vacuum triodes [18, 23].

In the following we will derive explicit expressions for $\bar{\kappa}$ in a number of geometries which give excellent approximations to the values obtained numerically. Let us also note that it should be possible to put our homogenization procedure on a rigorous footing using the methods of [22].

Homogenization procedure. At least formally, one can homogenize the fine-grained boundary condition by studying a boundary layer near $\partial\Omega$ and matching the boundary layer solution with the solution in the interior of the domain (for formal asymptotic studies of related problems, see, e.g., [34, 38, 39]). Given a point $\mathbf{x}_0 \in \partial\Omega$,

we choose the coordinates (x, y, z) to be the rescaled Cartesian coordinates in the vicinity of \mathbf{x}_0 aligned with the normal ν to $\partial\Omega$ at \mathbf{x}_0 :

$$(2.7) \quad z = -\varepsilon^{-1}\nu \cdot (\mathbf{x} - \mathbf{x}_0), \quad (x, y) = \varepsilon^{-1}\text{Proj}_{T(\mathbf{x}_0)}(\mathbf{x} - \mathbf{x}_0),$$

where $\text{Proj}_{T(\mathbf{x}_0)}(\mathbf{x} - \mathbf{x}_0)$ denotes the projection of a point \mathbf{x} onto the tangent plane $T(\mathbf{x}_0)$ to $\partial\Omega$ at \mathbf{x}_0 . Then, to leading order in ε , the problem (2.1)–(2.3) near the boundary reduces to

$$(2.8) \quad \Delta u = 0, \quad u|_{\partial\Omega_0} = v, \quad u_z|_{T(\mathbf{x}_0) \setminus \partial\Omega_0} = -g,$$

where $u = u(x, y, z)$ is defined and stays bounded in the upper half-space $z > 0$, $\partial\Omega_0$ is the rescaled version of $\partial\Omega_0^\varepsilon$ projected onto $T(\mathbf{x}_0)$, with $v = v(\mathbf{x}_0)$ and $g = g(\mathbf{x}_0)$ assumed independent of (x, y) . Boundedness of the solution should then imply that the limit $\lim_{z \rightarrow \infty} u(x, y, z)$ exists and is independent of (x, y) , depending only on \mathbf{x}_0 through v and g .

Unit cell of homogenization. Let us now further assume that in the limit $\varepsilon \rightarrow 0$ the set $\partial\Omega_0$ can be obtained by repeating periodically a unit cell $D \subset \mathbb{R}^2$ with an absorber at $D_0 \subset D$ almost everywhere in $\partial\Omega_0^\varepsilon$. Then it is easy to see that the solution of (2.8) can be expressed via the following unit cell problem:

$$(2.9) \quad \Delta \bar{u} = 0 \quad \text{in } D, \quad \nu \cdot \nabla \bar{u}|_{\partial D \times (0, \infty)} = 0,$$

$$(2.10) \quad \bar{u}|_{D_0 \times \{0\}} = 0, \quad \bar{u}_z|_{(D \setminus D_0) \times \{0\}} = -1,$$

where we assumed that D is in fact the Wigner–Seitz cell for the periodic problem. We also assume that D contains the origin in \mathbb{R}^2 . Now define

$$(2.11) \quad \bar{\kappa}^{-1} = \lim_{z \rightarrow \infty} \bar{u}(0, 0, z).$$

Then, by linearity of (2.8), we have $\lim_{z \rightarrow \infty} u(x, y, z) = v + \bar{\kappa}^{-1}g$.

Since ε does not enter (2.1), the homogenized version of this equation remains unchanged. On the other hand, we need to match the boundary data for this equation as \mathbf{x} approaches $\partial\Omega$ with the behavior of the solution of the unit cell problem at infinity. Matching the values of u for both solutions, we arrive at (2.4), with $\bar{\kappa}$ given by (2.11). Note that since \bar{u} is a harmonic function, $\nu \cdot \nabla \bar{u} = 0$ on $\partial D \times (0, \infty)$, and u is bounded, we have $\iint_D \bar{u}(x, y, z) \, dx dy = \text{const}$, independent of z . Hence we also get an alternative representation for $\bar{\kappa}$ in terms of the solution on $T(\mathbf{x}_0)$ only:

$$(2.12) \quad \bar{\kappa}^{-1} = \frac{1}{|D|} \iint_{D \setminus D_0} \bar{u}(x, y, 0) \, dx dy.$$

Stochastic interpretation. We now give a stochastic interpretation of the problem in (2.9) and (2.10) and demonstrate the meaning of the constant $\bar{\kappa}$ as the rescaled effective trapping rate for a Brownian particle over the surface $\partial\Omega_0$ [2, 3, 4]. Suppose that a Brownian particle with diffusion constant unity starts with equal probability at a point (x_0, y_0) anywhere in D on the $z = 0$ plane at $t = 0$. Under the assumptions of periodicity and symmetry of the unit cell, the survival probability $P(t)$ of the particle at time $t > 0$ can be found by constraining the particle to move in a semi-infinite cylinder $\Sigma_+ = D \times (0, +\infty)$ with reflecting boundary conditions on the sides. Note that the particle is immediately absorbed if $(x_0, y_0) \in D_0$.

To simplify matters further, one can restrict the particle to move within a finite cylinder $\Sigma_L = D \times (0, L)$, with L fixed and a reflecting boundary condition at $z = L$. Then the average lifetime of such a particle is $T = \int_0^\infty P(t) dt$ [13]. For $L \gg 1$ the average lifetime of the particle in Σ_L at long times behaves asymptotically as $T \simeq \kappa^{-1} L$ for some constant κ depending only on the geometry of D and D_0 [4]. This expression coincides with the exact result for the one-dimensional Brownian motion in the presence of a partially absorbing boundary condition at $z = 0$ with trapping rate κ .

To be more specific, consider the Green's function $G(x, y, z, t | x_0, y_0, 0, 0)$ for the Brownian particle in Σ_L starting at $(x_0, y_0) \in D$ on the $z = 0$ plane. When $(x_0, y_0) \notin D_0$, the Green's function satisfies

$$(2.13) \quad G_t = \Delta G, \quad G_z|_{(D \setminus D_0) \times \{0\}} = -\delta(x - x_0)\delta(y - y_0)\delta(t),$$

$$(2.14) \quad G_z|_{D \times \{L\}} = 0, \quad G|_{D_0 \times \{0\}} = 0, \quad \nu \cdot \nabla G|_{\partial D \times (0, L)} = 0.$$

The survival probability $P(t)$ is then obtained by integrating the Green's function over Σ_L and then averaging over $(x_0, y_0) \in D$. This should be compared with the solution of the one-dimensional problem with a partially absorbing boundary condition at $z = 0$:

$$(2.15) \quad \tilde{G}_t = \tilde{G}_{zz}, \quad \tilde{G}_z|_{z=0} = -\delta(t) + \kappa \tilde{G}|_{z=0}, \quad \tilde{G}_z|_{z=L} = 0.$$

Here $\tilde{G}(z, t | 0, 0)$ is the Green's function of a Brownian particle on an interval $(0, L)$ with a reflecting boundary condition at $z = L$ and a partially absorbing boundary condition at $z = 0$. Using backward Kolmogorov equation [13], the average lifetime of this particle is easily calculated to be

$$(2.16) \quad T = \frac{L}{\kappa}.$$

Thus, the constant κ in (2.15) can be associated with the value of $\lim_{L \rightarrow \infty} (T/L)$, where T is obtained from (2.13) and (2.14).

Now, to see how this picture is related to the homogenization limit introduced in (2.4) earlier, let us define $u = \lim_{\varepsilon \rightarrow 0} \varepsilon^{-1} G^\varepsilon$, where G^ε is the Green's function of the problem in which the absorber D_0 , the cell D , and the periodic lattice have been rescaled by ε . Then (2.4) corresponding to (2.13) and (2.14) reads

$$(2.17) \quad u_t = u_{zz}, \quad u(z, 0) = 0, \quad u(0, t) = \bar{\kappa}^{-1} \delta(t), \quad u_z(L, t) = 0.$$

Solving this boundary value problem with the aid of the Laplace transform, $U(z, s) = \int_0^\infty e^{-st} u(z, t) dt$, we find that

$$(2.18) \quad \int_0^L U(z, s) dz = \frac{\tanh L\sqrt{s}}{\bar{\kappa}\sqrt{s}},$$

which, up to the factor of ε , is the Laplace transform of the survival probability $P(t)$ to leading order. From this, the average lifetime of the particle can be found:

$$(2.19) \quad \varepsilon^{-1} T = \lim_{s \rightarrow 0} \int_0^L U(z, s) dz = \frac{L}{\bar{\kappa}},$$

which, in view of (2.5), is equivalent to (2.16). Note that in deriving (2.19) we took into account that the homogenized problem in (2.17) should be valid for $t \gg \varepsilon^2$,

the time it takes a particle to diffuse far away from the boundary on the scale of the absorbers, and that the transient for $t \lesssim \varepsilon^2$ does not contribute to the average lifetime in the limit $\varepsilon \rightarrow 0$. We point out, however, that most of the particles will be recaptured for $t \gg \varepsilon^2$, since $P(t) \sim \varepsilon/\sqrt{t} \ll 1$ for $\varepsilon^2 \ll t \ll 1$. However, only the particles that wander far away from the boundary contribute to T ; hence, it is the homogenized problem that governs the particle's *average* lifetime in the limit $\varepsilon \rightarrow 0$.

3. Numerical methods. We now describe our numerical approaches to the unit cell problem in (2.9) and (2.10). The Brownian dynamics algorithm used to obtain the effective trapping rate κ in [5] has been described previously [2]. Here we use a novel approach to this problem based on the concept of optimal grids, a recently proposed method for studying exterior elliptic boundary value problems [10, 11, 15]. Our numerical results are based on the latter method, but we also verified our results using stochastic simulations with the Brownian dynamics algorithm.

To recast the unit cell problem in the language of optimal grids, first we subtract the limit at infinity from \bar{u} ,

$$(3.1) \quad \tilde{u} = \bar{u} - \bar{\kappa}^{-1},$$

to ensure that $\tilde{u} \rightarrow 0$ as $z \rightarrow 0$ uniformly in D . Then \tilde{u} solves in $\Sigma_+ = D \times (0, \infty)$

$$(3.2) \quad \Delta \tilde{u} = 0, \quad \nu \cdot \nabla \tilde{u}|_{\partial D \times (0, \infty)} = 0, \quad \tilde{u}|_{D \times \{\infty\}} = 0,$$

$$(3.3) \quad \tilde{u}(x, y, 0) = v(x, y), \quad \tilde{u}_z(x, y, 0) = -g(x, y),$$

where $g(x, y) = 1$ in $D \setminus D_0$ and $v(x, y) = -\bar{\kappa}^{-1}$ in D_0 . Thus, what we need to do is reconstruct the partial Dirichlet data on D_0 from partial Neumann data on $D \setminus D_0$ in the considered boundary value problem. We note that this problem is not easily amenable to standard eigenfunction expansion techniques, since the boundary data consist of a mixture of Dirichlet and Neumann boundary conditions. This is why the optimal grid approach can be especially useful for this type of problem.

The method of optimal grids uses a judiciously chosen sequence of grid steps in a staggered discretization of the Laplacian in Σ_+ to approximate the Neumann-to-Dirichlet map $g \mapsto v$ for the boundary value problem in (3.2) and (3.3) on $D \times \{0\}$. As we will show below, this method in fact allows us to treat problems with mixed Neumann–Dirichlet-type boundary conditions equally well. The method can be briefly summarized as follows. Let us introduce the complete orthonormal basis of eigenfunctions of the transverse Laplacian $\Delta_\perp = \frac{\partial^2}{\partial x^2} + \frac{\partial^2}{\partial y^2}$ in D with Neumann boundary conditions on ∂D . Then we can write (3.2) as

$$(3.4) \quad \frac{d^2 \tilde{u}_l}{dz^2} - \lambda_l \tilde{u}_l = 0, \quad \frac{d\tilde{u}_l}{dz} \Big|_{z=0} = -g_l, \quad \tilde{u}_l(+\infty) = 0,$$

where $\tilde{u}_l = \tilde{u}_l(z)$, the values of $\lambda_l \geq 0$ are the eigenvalues of $-\Delta_\perp$, and the subscript l denotes the corresponding projections on the l th eigenfunction. A simple calculation shows that in terms of these projections the Neumann-to-Dirichlet map is simply (see, e.g., [37])

$$(3.5) \quad v_l = \tilde{u}_l(0) = F(\lambda_l) g_l, \quad F(\lambda) = \frac{1}{\sqrt{\lambda}}.$$

The function $F(\lambda)$ is usually referred to as the impedance function.

In the optimal grid approach, the impedance function $F(\lambda)$ is approximated by a rational function $F_n(\lambda)$ of order $n - 1$ by n . This rational function is chosen in such a way that $F_n(\lambda)$ is in a certain sense the best possible approximation to the original impedance function $F(\lambda)$ on an appropriate spectral interval $\lambda \in [\lambda_{\min}, \lambda_{\max}]$ [10, 11, 15]. The resulting optimal rational approximant can be written as a continued fraction:

$$(3.6) \quad F_n(\lambda) = \frac{1}{\lambda h_0 + \frac{1}{h_{1/2} + \frac{1}{\lambda h_1 + \cdots + \frac{1}{h_{n-1/2}}}}},$$

where all $h_i > 0$. A remarkable observation that stands behind the method of optimal grids is the fact that the impedance function $F_n(\lambda)$ in (3.6) is also the impedance function of the *discrete* problem

$$(3.7) \quad \frac{1}{h_i} \left(\frac{\tilde{u}_{i+1}^l - \tilde{u}_i^l}{h_{i+1/2}} - \frac{\tilde{u}_i^l - \tilde{u}_{i-1}^l}{h_{i-1/2}} \right) - \lambda_l \tilde{u}_i^l = 0, \quad i = 0, 1, \dots, n-1.$$

More precisely, if we set $(\tilde{u}_0^l - \tilde{u}_{-1}^l)/h_{-1/2} = -g_l$ and $\tilde{u}_n^l = 0$, then it is not difficult to show that $\tilde{u}_0^l = F_n(\lambda_l)g_l$, where $F_n(\lambda)$ is given by (3.6). This suggests using the following semidiscrete scheme for approximating the Neumann-to-Dirichlet map arising from (3.2):

$$(3.8) \quad \frac{1}{h_i} \left(\frac{\tilde{u}_{i+1} - \tilde{u}_i}{h_{i+1/2}} - \frac{\tilde{u}_i - \tilde{u}_{i-1}}{h_{i-1/2}} \right) + \Delta_{\perp} \tilde{u}_i = 0, \quad \frac{\tilde{u}_0 - \tilde{u}_{-1}}{h_{-1/2}} = -g, \quad \tilde{u}_n = 0,$$

where now $\tilde{u}_i = \tilde{u}_i(x, y)$ and $g = g(x, y)$, with $(x, y) \in D$ and a Neumann boundary condition on ∂D . To obtain a fully discrete problem, one should then use any convenient conservative scheme (e.g., the usual five-point stencil if D is a rectangle) to discretize Δ_{\perp} in D .

This numerical procedure possesses several advantages. First, the obtained discrete problem can be treated efficiently using the conjugate gradient method because of the sparse symmetric matrices arising in (3.8). On the other hand, due to the exponential superconvergence of the optimal rational approximation [15] with increasing n one needs very few nodes (in practice, only 4–6 nodes are often sufficient) to get a good uniform accuracy of the approximation of the Neumann-to-Dirichlet map on the entire relevant spectral interval, essentially preserving the quasi-two-dimensional nature of the problem. Actually, for n sufficiently large the steps h_i of the grid obtained from the optimal rational approximant that are suitable for the fully discrete problem become asymptotically close to those of the *optimal geometric grid*, whose steps are explicitly given by [15]

$$(3.9) \quad h_0 = \frac{h_{\perp}}{1 + e^{\pi/(2\sqrt{n})}}, \quad h_{1/2} = h_{\perp}, \\ h_{i+1/2} = h_{i-1/2} e^{\pi/\sqrt{n}}, \quad h_i = \sqrt{h_{i+1/2} h_{i-1/2}},$$

where h_{\perp} is the characteristic grid size of the discretization of the Laplacian Δ_{\perp} in D . In the following, we will use the steps of the optimal geometric grid in discretizing the

problem in the direction of z . Note that the number of grid steps n can be estimated by considering the effective “length” $L_z = \sum_{i=0}^{n-1} h_{i+1/2}$ of the grid in the z direction:

$$(3.10) \quad L_z = h_\perp \frac{e^{\pi\sqrt{n}} - 1}{e^{\frac{\pi}{\sqrt{n}}} - 1}.$$

By choosing $L_z \gg \text{diam}(D)$, we assure that the grid accurately resolves all the scales of the problem.

This method needs to be adapted for the case of the mixed boundary condition in (3.2). Since the solution \tilde{u}_n decays rapidly for large n , the flux through the n th node of the optimal grid can be assumed to be zero. So, as a first step we will replace the Dirichlet boundary condition in (3.8) with a reflecting boundary condition: $\tilde{u}_{n+1} = \tilde{u}_{n-1}$, $h_{n+1/2} = h_{n-1/2}$, and set $h_n = 0$ (consistent with the original assumption $\tilde{u}_n = 0$). We can also replace the inhomogeneous Neumann boundary condition for $i = 0$ with the Dirichlet boundary condition for \tilde{u}_0 inside D_0 . Still, the constant $\bar{\kappa}^{-1}$ we need to choose there is unknown. Nevertheless, because we can add an arbitrary constant to \tilde{u} in (3.8), we can simply set $\tilde{u}_0 = 0$ in D_0 and, after obtaining the solution, identify $\bar{\kappa}^{-1}$ with the value of \tilde{u}_n somewhere in D . This is how the value of $\bar{\kappa}$ is extracted from the solution of the mixed boundary value problem on the optimal grid. Note that a good indicator of the proper choice of n in the problem discretization is smallness of variation of \tilde{u}_n across D .

4. Results. Now we present the results of the numerical solution of the unit cell problem of homogenization for a number of unit cell geometries. We will first consider the case in which the absorbers and emitters form alternating arrays of stripes, for which an exact solution is available. We will then analyze hexagonal and square lattices of disk-shaped absorbers or emitters (see Figure 4.1). In all cases, the geometric factor $\bar{\kappa}$ is computed as a function of σ , the surface area fraction covered by the absorbers.

Our findings can be summarized using a few simple approximation formulas accurately describing the data for most of the values of σ . In the case of periodic arrays of disk-shaped absorbers of unit radius the dependence $\bar{\kappa}(\sigma)$ is well approximated by the following formula:

$$(4.1) \quad \bar{\kappa}(\sigma) \approx \frac{4\sigma(1 + A\sigma^{1/2} - B\sigma^2)}{\pi(1 - \sigma)^2},$$

where the constants A and B depend on the geometry of D . For hexagonal and square lattices we have $A = 1.49, 1.02$ and $B = 0.92, 0.46$, respectively, which approximate the data obtained numerically within 3% and 6% error in the intervals $0.01 \leq \sigma \leq 0.81$ and $0.01 \leq \sigma \leq 0.63$, respectively. These coefficients differ somewhat from the fits of [5] based on earlier, less accurate Brownian dynamics data. Let us note, however, that the fits to the numerical data are quite insensitive to changes in the coefficients A and B .

For comparison, we get $A = 1.37$ and $B = 0.37$ for a disk-shaped absorber of radius one in a cylinder with reflecting boundary conditions. With these values of A and B , (4.1) is valid for the cylinder within 1% error in the interval $0.001 \leq \sigma \leq 0.9$ and within 3% for all the available data. Note that the data for both hexagonal and square lattices differ by no more than 25% from the solution for the cylinder for the entire range of σ of the simulations, and the agreement increases rapidly when σ is decreased. On the other hand, the value of $\bar{\kappa}$ begins to deviate from the asymptotic

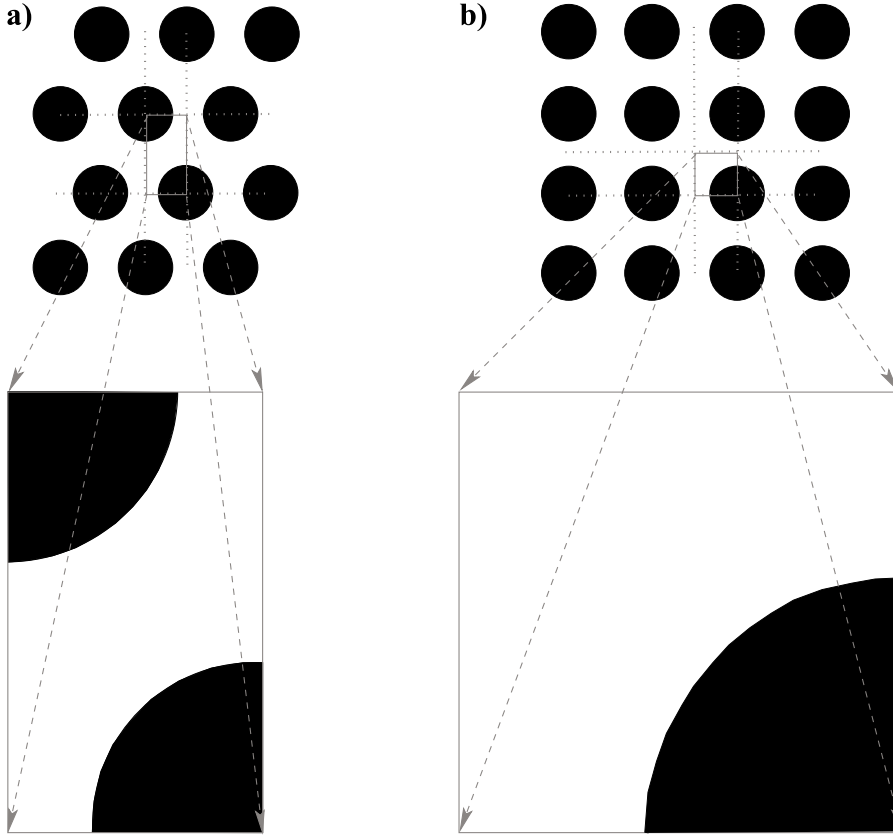


FIG. 4.1. The geometry of the unit cell for hexagonal (a) and square (b) lattices. The outer boundary of the rectangle is reflecting. The lines of symmetry are shown by dotted lines.

value $\bar{\kappa} \simeq 4\sigma/\pi$ noticeably already for $\sigma \gtrsim 0.01$. In addition, (4.1) also gives an improvement for fitting the data for randomly distributed absorbers [4], with the values of $A = 0.34$ and $B = -0.58$ giving a 5% error within the interval $0 \leq \sigma \leq 0.5$. Note that there is a more noticeable difference with the cylinder data for random absorbers compared to periodic geometries, even for small σ . For example, at $\sigma = 0.5$ the value of $\bar{\kappa}$ for random absorbers is about 30% less than that for the cylinder, while the latter is virtually indistinguishable from the value for the hexagonal lattice.

We next consider the “inverted” situation, namely, when the absorber occupies the *exterior* of the unit disk in a hexagonal or square unit cell. In this case we found that the expression

$$(4.2) \quad \bar{\kappa}(\sigma) \approx \frac{\pi}{(1 - \sigma) \ln(2.76 + 1.03\sigma^{-1})}$$

fits both sets of data within 5% in the whole range of σ . We also computed the dependence $\bar{\kappa}(\sigma)$ for a cylinder with a disk-shaped emitter of unit radius in the center. We found that this dependence agrees with (4.2) within the accuracy of 1% in the interval $0.02 \leq \sigma \leq 0.98$ and within 4% for all the available data. In fact, we found that the

data for both the hexagonal and the square cells are virtually indistinguishable from the data for the cylinder.

Finally, in the case of absorbing stripes of width 2 alternating with the emitting stripes we recover the formula from the exact solution obtained by Moizhes [23] (also see the appendix):

$$(4.3) \quad \bar{\kappa}(\sigma) = -\frac{\pi\sigma}{2 \ln \sin\left(\frac{\pi\sigma}{2}\right)}.$$

This formula can be used to test the performance of our numerical method.

4.1. Periodic absorbing stripes. Let us start by considering the problem with the absorbers in the form of periodic stripes of width 2 alternating with the emitters of width $2(\sigma^{-1} - 1)$. We discretize Δ_{\perp} in (3.8) on half-period $L = \sigma^{-1}$, using the standard three-point stencil on the grid $x_j = jh_{\perp}$, $j = 0, 1, \dots, m$:

$$(4.4) \quad h_{\perp}^2 \Delta_{\perp} \tilde{u}_i(x_j) \approx \tilde{u}_i(x_{j+1}) + \tilde{u}_i(x_{j-1}) - 2\tilde{u}_i(x_j),$$

with reflecting boundary conditions at $j = 0$ and $j = m$ and with $h_{\perp} = L/m$. The resulting discrete problem can be conveniently represented using an electrical analogy as a resistor network shown in Figure 4.2 [7]. The bottom left nodes, $i = 0$, $j \leq \sigma m$, are maintained at zero “potential,” and the right bottom nodes, $i = 0$, $j > \sigma m$, are those through which a unit current is injected. The vertical edges connecting the i th and the $(i + 1)$ th rows correspond to resistors with resistance $h_{i+1/2}$, and the horizontal edges between the node (i, j) and $(i, j + 1)$ correspond to resistors with resistance h_{\perp}^2/h_i .

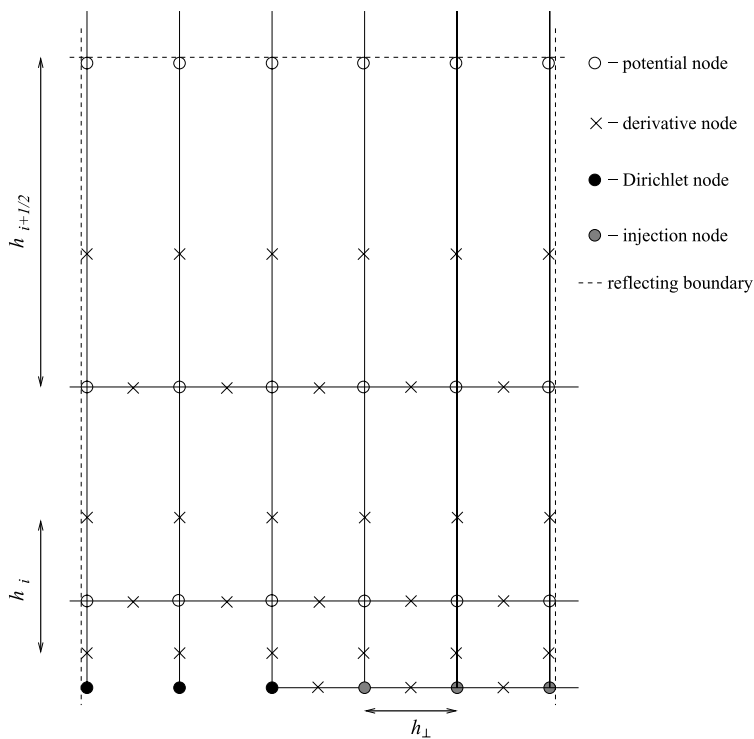


FIG. 4.2. Representation of the grid in the form of a resistor network (see text for details).

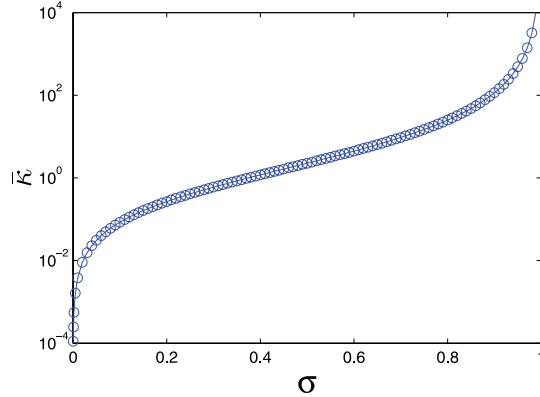


FIG. 4.3. The dependence $\bar{\kappa}(\sigma)$ for absorbing stripes of width 2 alternating with emitting stripes, obtained from the numerical solution of (2.9) and (2.10). Circles show the data points; the solid line is the result of plotting (4.3).

The result of the numerical solution of the unit cell problem with $n = 10$ and $m = 1000$ and its comparison with the exact solution are shown in Figure 4.3. Note that when $\sigma \rightarrow 0$ we have asymptotically $\bar{\kappa} \simeq \pi\sigma/(2 \ln \sigma^{-1})$, which can be easily seen from the electrostatic analogy and (2.12), once it is noted that the absorbers each carry “charge” $-4\sigma^{-1}$, and so for $\sigma \ll 1$ the potential \bar{u} at distance r from the center of the nearest absorber is asymptotically $\bar{u}(r, 0) \simeq -(2/\pi\sigma) \ln r$, and $\bar{\kappa} \simeq 1/u(\sigma^{-1}, 0)$. On the other hand, when $\sigma \rightarrow 1$, we have asymptotically $\bar{\kappa} \simeq (4/\pi)(1 - \sigma)^{-2}$; see the appendix. Our numerical results agree with the exact solution to within 0.3% in the interval $0.1 \leq \sigma \leq 0.8$. Also, the error is at most 1% for $0.01 \leq \sigma \leq 0.94$ and within 3% for the entire data set. Let us emphasize that our numerical solution accurately captures 8(!) orders of magnitude of $\bar{\kappa}(\sigma)$ for the stripe geometry.

4.2. Disk absorbers in cylindrical and periodic geometries. We will now study a particular case in which D_0 is a unit disk and D is a concentric disk of radius $R = \sigma^{-1/2}$. Because of the radial symmetry, this problem is essentially two-dimensional and may therefore be more accurately resolved. On the other hand, we will also show that the solution of the unit cell problem on a cylinder gives an excellent approximation to that on a hexagonal cell, as should be expected.

Due to the radial symmetry, we need only consider $\bar{u} = \bar{u}(r, z)$, with $\Delta_{\perp} = \partial_r^2 + r^{-1}\partial_r$, and the boundary conditions $\bar{u}_r(0, z) = \bar{u}_r(R, z) = 0$, $\bar{u}(r, 0) = 0$, $0 < r < 1$, and $\bar{u}_z(r, 0) = -1$, $1 < r < R$. The transverse Laplacian in (3.8) is then discretized with a three-point stencil using harmonic averaging on a uniform grid $r_j = jh_{\perp}$, $j = 1, 2, \dots, m$ [33]:

$$(4.5) \quad h_{\perp}^2 \Delta_{\perp} \tilde{u}_i(r_j) \approx \frac{\tilde{u}_i(r_{j-1})}{j \ln(\frac{j}{j-1})} + \frac{\tilde{u}_i(r_{j+1})}{j \ln(\frac{j+1}{j})} - \left(\frac{1}{j \ln(\frac{j}{j-1})} + \frac{1}{j \ln(\frac{j+1}{j})} \right) \tilde{u}_i(r_j),$$

where $h_{\perp} = R/m$. To satisfy the boundary conditions at $r = 0$ and $r = R$, we set the flux from the left to all $j = 1$ nodes to zero and put a reflecting boundary condition at $j = m$. The corresponding resistor network in Figure 4.2 will have the first $\sigma^{1/2}m$ bottom-left nodes at zero potential, with the rest of the bottom nodes being injection nodes. The vertical edges connecting the i th and the $(i + 1)$ th rows correspond to

resistors with resistance $h_{i+1/2}/j$, and the horizontal edges between the node (i, j) and $(i, j + 1)$ now correspond to resistors with resistance $\ln(\frac{j+1}{j})h_{\perp}^2/h_i$.

We used this discretization scheme to construct the numerical solution of the unit cell problem of homogenization in the considered geometry. Let us note that the obtained scheme is still first order in h_{\perp} due to the presence of a combination of inhomogeneous Neumann and homogeneous Dirichlet boundary conditions. Nevertheless, the scheme gives an accuracy which is adequate for our purposes, while being able to resolve over four orders of magnitude of the variation of $\bar{\kappa}$ as the value of σ is varied. In the results presented below we used $m = 1000$ and $n = 10$ to compute the value of $\bar{\kappa}$ to within 1% error in the range $0.001 \lesssim \sigma \lesssim 0.94$.

The results of the numerical solution of this problem are presented in Figure 4.4 both on the logarithmic (a) and linear (b) scale. The fitting form in (4.1) is obtained using careful analysis of our data, specifically its behavior for $\sigma \simeq 0$ and $\sigma \simeq 1$. Note that in the limit $\sigma \rightarrow 0$ we recover the well-known asymptotic result $\bar{\kappa} \simeq 4\sigma/\pi$ for small absorber area fractions [6, 21, 25, 34, 39]. By further analyzing our data, we were able to extract the next-order correction to the leading-order asymptotic formula mentioned above for $\sigma \ll 1$; this term is associated with the coefficient A in (4.1). Specifically, we plotted the expression $\pi\bar{\kappa}(\sigma)(1-\sigma)^2/(4\sigma) - 1$ on the log-log plot; see Figure 4.5. From the known $\sigma \ll 1$ asymptotics this expression goes to zero as $\sigma \rightarrow 0$. One can then see from Figure 4.5 (of course, one needs to discard the data for very small values of σ as insufficiently accurate) that in the range $0.005 \lesssim \sigma \lesssim 0.2$ the data can be well approximated with a straight line with slope $1/2$, suggesting that the next-order correction to the $\sigma \rightarrow 0$ asymptotics gives $\bar{\kappa}(\sigma) \simeq (4\sigma/\pi)(1 + A\sigma^{1/2})$. At the same time, one can see that as $\sigma \rightarrow 1$, the expression above approaches 1, in agreement with the asymptotic formula $\bar{\kappa} \simeq (8/\pi)(1-\sigma)^{-2}$ obtained in the appendix.

We then found that the best fit to the data in terms of the relative error for the entire range of σ 's is obtained by using the expression in (4.1) which combines the higher-order correction term $A\sigma^{1/2}$ discussed earlier with an empirical term $B\sigma^2$. The power 2 in the latter was found to be roughly optimal for fitting all our data (including that for hexagonal and square cells) up to $\sigma \simeq 1$.

To discretize the problems in periodic geometries, we used the standard five-point stencil to approximate $\Delta_{\perp}u$ on an $m_1 \times m_2$ square grid with $m_2/m_1 \approx \sqrt{3}$ for the

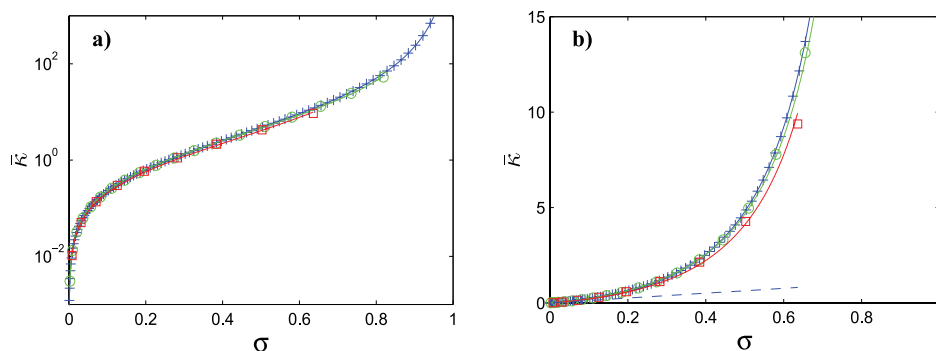


FIG. 4.4. The dependence $\bar{\kappa}(\sigma)$ obtained from the numerical solution of (2.9) and (2.10) for the unit disk absorber in a cylindrical (crosses), hexagonal (circles), and square (squares) unit cell. The lines containing these symbols are the fits given by (4.1). In (a), the data are shown on the log-linear scale; in (b) the same data are plotted on a linear plot. The dashed line in (b) is the asymptotic expression $\bar{\kappa} \simeq 4\sigma/\pi$, valid when $\sigma \rightarrow 0$.

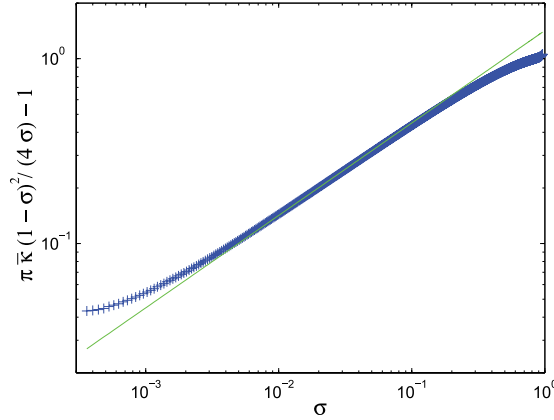


FIG. 4.5. The dependence $\bar{\kappa}(\sigma)$ for the cylinder replotted. The straight line is $1.42\sigma^{1/2}$.

hexagonal cell and $m_1 = m_2$ for the square cell and used discrete no-flux boundary conditions. We used symmetry to transform the problem for both the hexagonal and the square lattice so that the computational domain in the (x, y) plane is a rectangle (see Figure 4.1). The results of the computation of $\bar{\kappa}(\sigma)$ for both geometries are shown in Figure 4.4. In both cases, we used $n = 8$ and $m_1 = 200$. As was already mentioned, our main observation is that the results for the periodic geometries differ little from those for the cylinder with the same value of σ . In particular, the asymptotic behaviors of $\bar{\kappa}(\sigma)$ as $\sigma \rightarrow 0$ and $\sigma \rightarrow 1$ essentially coincide with those of the cylindrical cell.

4.3. Disk emitter in cylindrical and periodic geometries. Now we invert the roles of the absorbers and emitters from the previous section and consider the case of the emitter in the form of a unit disk. The numerics are the same as above, with the Neumann and Dirichlet nodes on the computational boundary interchanged. The results of the numerical solution of the unit cell problem for cylindrical, hexagonal, and square cells are shown in Figure 4.6 and essentially all fall on the curve given by (4.2).

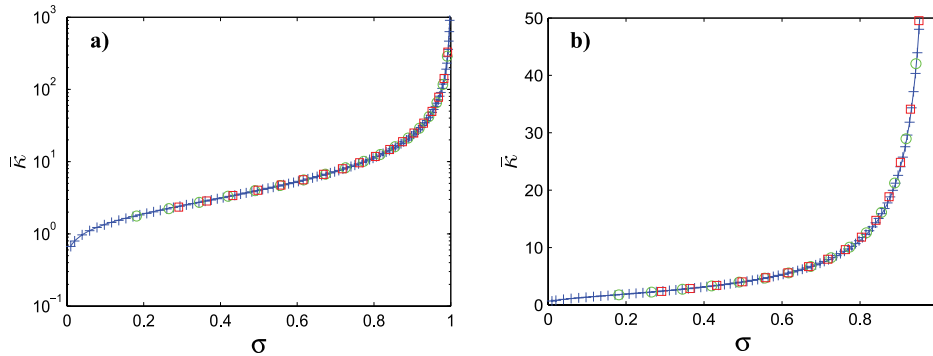


FIG. 4.6. The dependence $\bar{\kappa}(\sigma)$ obtained from the numerical solution of (2.9) and (2.10) for the unit disk emitter in a cylindrical (crosses), hexagonal (circles), and square (squares) unit cell. The solid line is the fit given by (4.2). In (a), the data are shown on the log-linear scale, in (b) the same data are plotted on a linear plot.

The fitting form used in (4.2) is essentially an interpolation from the limit behaviors for $\sigma \rightarrow 0$ and $\sigma \rightarrow 1$ for a disk-shaped emitter of unit radius in a disk of radius $R = (1 - \sigma)^{-1/2}$. When $\sigma \simeq 1$, we are essentially dealing with an emitter on an absorbing plane; hence the distribution of \bar{u} solving (2.9) and (2.10) will approach a limit as $R \rightarrow \infty$. Then from (2.12) we infer that $\bar{\kappa} \sim (1 - \sigma)^{-1}$ as $\sigma \rightarrow 1$. On the other hand, for $\sigma \rightarrow 0$ the absorber degenerates into a thin rim of width $\sigma/2$ along the outer boundary of D and will carry a linear “charge” density $-2\pi/(2\pi R) \simeq -1$ (using the electrostatic analogy). Therefore, one expects, taking into account a reflecting boundary condition at $r = R$, that $\bar{u}(r, 0) \simeq -(1/\pi) \ln\{\sigma(R - r)\}$, and so $\bar{\kappa} \simeq \pi/\ln \sigma^{-1}$ as $\sigma \rightarrow 0$, in agreement with (4.2).

5. Conclusions. To conclude, we have developed a homogenization procedure that allows us to treat reaction-diffusion problems in which a fine-grained boundary consists of portions that inject a strong flux of particles into the system alternating with portions that work as traps. A novel feature of the homogenization procedure is that in the homogenization limit the effective boundary condition becomes of inhomogeneous *Dirichlet* type and is related to the Neumann data on the boundary via a geometric factor that depends only on the shape of the unit cell of homogenization. To compute this geometric factor, one needs to solve an elliptic boundary value problem in a semi-infinite domain.

To find the geometric factor numerically for a number of geometries, we used the method of geometric optimal grids to discretize the unit cell problem. This method proved to be very effective in resolving the multiscale nature of the problem, as the geometric factor changes by many orders of magnitude upon changes in the emitter to absorber area fraction. Our numerical results are in excellent agreement with the available exact solution and the asymptotic behaviors found by us for large and small fractions of surface area occupied by the absorbers.

Our results can be naturally extended in a number of ways. First, it is possible to extend our result to the case in which ideal absorbers are replaced by partial absorbers; i.e., instead of the Dirichlet data on the absorbers one would prescribe mixed boundary conditions. This problem is important for cell signaling applications, since in reality cell surface receptors do not always work as perfect absorbers [2, 24, 40]. Moreover, in many problems related to cell signaling the same surface can play the role of an absorber or emitter depending on the state of the individual cell in a layer. Also, a related extension is to consider a heterogeneous layer consisting of cells of different types, with different absorption and emission properties.

Second, it would be interesting to consider the situation in which signaling is coupled to changes in the state of the cell in a cell layer; this is, of course, what happens in real tissues [29, 30, 31, 32]. One point to investigate here is how the solution of the homogenized problem couples back to the intracellular dynamics. One intriguing possibility is that the cell might be able to read the *flux* of the signaling molecules coming onto its surface. Indeed, when the cells in the layer act as nearly perfect absorbers, most of the signaling molecules in the layer of extracellular space above the cell will be bound to the cell surface receptors. But at the same time the number of signal-receptor complexes will be determined by the rate of signal-induced receptor endocytosis [2, 24, 40], which will be balanced by the net flux of the signaling molecules coming to the cell from the extracellular medium. Therefore, under certain conditions one would expect the number of receptor-bound signaling molecules to be proportional to the surface flux of free signaling molecules.

Finally, on the numerical side, one could also consider the problem in which the

absorbers and the emitters do not lie on a plane in the homogenization limit but instead form a short-scale topography. To solve the unit cell problem of homogenization in such a setup, one could combine, say, a finite volume discretization of the space between the peaks of the topography with an optimal geometric grid above it. Of course, our method is not limited by a particular choice of the geometry of the cell, and so it can be easily applied to cells of arbitrary shapes. One can further improve the accuracy and efficiency of our method by using discretization schemes aligned with the boundaries of the absorbers; this work is currently in progress [27].

Appendix A. Behavior of $\bar{\kappa}(\sigma)$ for absorbing stripes as $\sigma \rightarrow 1$. We can estimate the behavior of $\bar{\kappa}$ for stripes as $\sigma \rightarrow 1$ directly by analyzing the formula in (4.3). This formula was obtained by Moizhes from the exact solution of this problem, which is given by [23]

$$(A.1) \quad \bar{u}(x, y) = \operatorname{Re} w(x + iy), \quad w(z) = iz + \frac{2i}{\pi\sigma} \arccos \left(\frac{\sin \left(\frac{\pi\sigma z}{2} \right)}{\sin \left(\frac{\pi\sigma}{2} \right)} \right).$$

On the other hand, it is also instructive to derive this asymptotic result without resorting to the solution in (A.1), since it shows how to find the asymptotic behavior as $\sigma \rightarrow 1$ for more general stripe-like geometries.

So, first consider bounded solutions of the following auxiliary problem in \mathbb{R}^2 :

$$(A.2) \quad \Delta u = 0, \quad y > 0, \quad u(x, 0) = 0, \quad |x| > a, \quad u_y(x, 0) = -1, \quad |x| < a.$$

It is not difficult so see that the exact solution to this problem is

$$(A.3) \quad u(x, y) = \operatorname{Re} u_0(x + iy), \quad u_0(z) = \sqrt{a^2 - z^2} + iz,$$

with the usual branch cut $(-\infty, -a] \cup [a, +\infty)$ on the real axis. In particular, when $r = \sqrt{x^2 + y^2} \rightarrow \infty$, with $\arg(x + iy)$ fixed, we have

$$(A.4) \quad u = O\left(\frac{a}{r}\right), \quad y \neq 0, \quad u_y = O\left(\frac{a^2}{r^2}\right), \quad y = 0.$$

Therefore, to within $O(a^2/L^2)$ the solution \bar{u} for the $2L$ -periodic array of stripes can be taken to be a superposition of the solutions in (A.3):

$$(A.5) \quad \bar{u}(x, y) \simeq \sum_{n=-\infty}^{\infty} \operatorname{Re} u_0(x + iy - (2n + 1)L).$$

To obtain the leading-order behavior of $\bar{\kappa}$, we use (2.12) and average \bar{u} over half-period

$$(A.6) \quad \bar{\kappa}^{-1} = \frac{1}{L} \int_0^L \operatorname{Re} u_0(x) dx = \frac{\pi a^2}{4L}.$$

In view of the fact that $1 - \sigma = a/L$ and $L = \sigma^{-1}$, we obtain

$$(A.7) \quad \bar{\kappa} \simeq \frac{4}{\pi(1 - \sigma)^2}, \quad \sigma \rightarrow 1.$$

In the case of an infinite cylinder with radius $R \rightarrow 1^+$ the leading-order solution can be similarly constructed to be $\bar{u}(r, z) \simeq \operatorname{Re} u_0(R - r - iz)$, with $a = R - 1$. So, averaging this expression over $z = 0$, we obtain

$$(A.8) \quad \bar{\kappa}^{-1} = \frac{2}{R^2} \int_0^R \operatorname{Re} u_0(r, 0) r dr = \frac{a^2(3\pi R - 4a)}{6R^2}.$$

From this and the fact that $R = \sigma^{-1/2}$, we obtain to leading order

$$(A.9) \quad \bar{\kappa} = \frac{8}{\pi(1-\sigma)^2}, \quad \sigma \rightarrow 1.$$

Acknowledgment. The authors would like to acknowledge multiple valuable discussions with A. M. Berezhkovskii and V. Druskin.

REFERENCES

- [1] N. ANSINI, *The nonlinear sieve problem and applications to thin films*, *Asymptot. Anal.*, 39 (2004), pp. 113–145.
- [2] L. BATSILAS, A. M. BEREZHKOVSII, AND S. Y. SHVARTSMAN, *Stochastic model of autocrine and paracrine signals in cell culture assays*, *Biophys. J.*, 85 (2003), pp. 3659–3665.
- [3] A. M. BEREZHKOVSII, L. BATSILAS, AND S. Y. SHVARTSMAN, *Ligand trapping in epithelial layers and cell cultures*, *Biophys. Chem.*, 107 (2004), pp. 221–227.
- [4] A. M. BEREZHKOVSII, YU. A. MAKHNOVSII, M. I. MONINE, V. YU. ZITSERMAN, AND S. Y. SHVARTSMAN, *Boundary homogenization for trapping by patchy surfaces*, *J. Chem. Phys.*, 121 (2004), pp. 11390–11394.
- [5] A. M. BEREZHKOVSII, M. I. MONINE, C. B. MURATOV, AND S. Y. SHVARTSMAN, *Homogenization of boundary conditions for surfaces with regular arrays of traps*, *J. Chem. Phys.*, 124 (2006), 036103.
- [6] H. C. BERG AND E. M. PURCELL, *Physics of chemoreception*, *Biophys. J.*, 20 (1977), pp. 193–219.
- [7] E. B. CURTIS AND J. A. MORROW, *Inverse Problems for Electrical Networks*, World Scientific, Singapore, 2000.
- [8] A. DAMLAMIAN, *Le problème de la passoire de Neumann*, *Rend. Sem. Mat. Univ. Politec. Torino*, 43 (1985), pp. 427–450.
- [9] T. DEL VECCHIO, *The thick Neumann’s sieve*, *Ann. Mat. Pura Appl. (4)*, 147 (1987), pp. 363–402.
- [10] V. DRUSKIN, *Spectrally Optimal Finite Difference Grids in Unbounded Domains*, Schlumberger-Doll Research Notes, EMG–002–97–22, Schlumberger-Doll Research Center, Cambridge, MA, 1997.
- [11] V. DRUSKIN AND S. MOSCOW, *Three-point finite difference schemes, Padé and the spectral Galerkin method. I. One-sided impedance approximation*, *Math. Comp.*, 71 (2001), pp. 995–1019.
- [12] O. K. DUDKO, A. M. BEREZHKOVSII, AND G. H. WEISS, *Rate constant for diffusion-influenced ligand binding to receptors of arbitrary shape on a cell surface*, *J. Chem. Phys.*, 121 (2004), pp. 1562–1565.
- [13] C. W. GARDINER, *Handbook of Stochastic Methods for Physics, Chemistry, and the Natural Sciences*, Springer-Verlag, New York, 1997.
- [14] S. HEINZE, *Wave solutions to reaction-diffusion systems in perforated domains*, *Z. Anal. Anwendungen*, 20 (2001), pp. 661–676.
- [15] D. INGERMAN, V. DRUSKIN, AND L. KNIZHNERMAN, *Optimal finite difference grids and rational approximations of the square root. I. Elliptic problems*, *Comm. Pure Appl. Math.*, 53 (2000), pp. 1039–1066.
- [16] N. M. JUHASZ AND W. M. DEEN, *Electrochemical measurements of mass-transfer at surfaces with discrete reactive areas*, *AIChE J.*, 39 (1993), pp. 1708–1715.
- [17] R. V. KOHN AND V. V. SLASTIKOV, *Geometrically constrained walls*, *Calc. Var. Partial Differential Equations*, 28 (2007), pp. 33–57.
- [18] V. S. LUKOSHKOV, *Some electrostatic properties of grid electrodes*, *Izv. Akad. Nauk SSSR Ser. Fiz.*, 8 (1944), pp. 243–247 (in Russian).
- [19] YU. A. MAKHNOVSII, A. M. BEREZHKOVSII, AND V. YU. ZITSERMAN, *Homogenization of boundary conditions on surfaces randomly covered by patches of different sizes and shapes*, *J. Chem. Phys.*, 122 (2005), 236102.
- [20] V. A. MARCHENKO AND E. YA. KHRUSLOV, *Boundary-value problems with fine-grained boundary*, *Mat. Sb.*, 65 (1964), pp. 458–472.
- [21] V. A. MARCHENKO AND E. YA. KHRUSLOV, *Boundary Value Problems in Domains with a Fine-Grained Boundary*, *Naukova Dumka*, Kiev, Russia, 1974 (in Russian).
- [22] V. A. MARCHENKO AND E. YA. KHRUSLOV, *Homogenization of Partial Differential Equations*, *Progr. Math. Phys.* 46, Birkhäuser Boston, Boston, MA, 2006.

- [23] B. YA. MOIZHES, *Averaged electrostatic boundary conditions for metallic meshes*, Zh. Tekh. Fiz., 25 (1955), pp. 167–176 (in Russian).
- [24] M. I. MONINE, A. M. BEREZHKOVSII, E. J. JOSLIN, H. S. WILEY, D. A. LAUFFENBURGER, AND S. Y. SHVARTSMAN, *Ligand accumulation in autocrine cell cultures*, Biophys. J., 88 (2005), pp. 2384–2390.
- [25] F. MURAT, *The Neumann sieve*, in Nonlinear Variational Problems (Isola d’Elba, 1983), Res. Notes in Math. 127, Pitman, Boston, MA, 1985, pp. 24–32.
- [26] H. G. OTHMER, *Synchronized and differentiated modes of cellular dynamics*, in Dynamics of Synergetic Systems (Proc. Internat. Sympos. Synergetics, Bielefeld, 1979), Springer Ser. Synergetics 6, Springer-Verlag, Berlin, 1980, pp. 191–204.
- [27] F. POSTA, C. B. MURATOV, AND S. Y. SHVARTSMAN, in preparation.
- [28] S. PRAGER AND H. L. FRISCH, *Interaction between penetration sites in diffusion through thin membranes*, J. Chem. Phys., 62 (1975), pp. 89–91.
- [29] M. PŘIBYL, C. B. MURATOV, AND S. Y. SHVARTSMAN, *Discrete models of autocrine cell communication in epithelial layers*, Biophys. J., 84 (2003), pp. 3624–3635.
- [30] M. PŘIBYL, C. B. MURATOV, AND S. Y. SHVARTSMAN, *Long-range signal transmission in autocrine relays*, Biophys. J., 84 (2003), pp. 883–896.
- [31] G. T. REEVES, C. B. MURATOV, T. SCHÜPBACH, AND S. Y. SHVARTSMAN, *Quantitative models of developmental pattern formation*, Devel. Cell, 11 (2006), pp. 289–300.
- [32] G. T. REEVES, R. KHALIFA, D. E. KLEIN, M. A. LEMMON, AND S. Y. SHVARTSMAN, *Computational analysis of EGFR inhibition by Argos*, Devel. Biol., 284 (2005), pp. 523–535.
- [33] A. A. SAMARSKII, *The Theory of Difference Schemes*, Monogr. Textbooks Pure Appl. Math. 240, Marcel Dekker, New York, 2001.
- [34] E. SÁNCHEZ-PALENCIA, *Boundary value problems in domains containing perforated walls*, in Nonlinear Partial Differential Equations and Their Applications, Collège de France Seminar, Vol. III (Paris, 1980/1981), Res. Notes in Math. 70, Pitman, Boston, MA, 1982, pp. 309–325.
- [35] D. SHOUP AND A. SZABO, *Role of diffusion in ligand-binding to macromolecules and cell-bound receptors*, Biophys. J., 40 (1982), pp. 33–39.
- [36] A. SZABO AND R. ZWANZIG, *Chronoamperometric current at a random ensemble of microdisk electrodes*, J. Electroanalytical Chem., 314 (1991), pp. 307–311.
- [37] M. E. TAYLOR, *Partial Differential Equations II: Qualitative Studies of Linear Equations*, Springer-Verlag, Berlin, 1996.
- [38] M. J. WARD AND J. B. KELLER, *Nonlinear eigenvalue problems under strong localized perturbations with applications to chemical reactors*, Stud. Appl. Math., 85 (1991), pp. 1–28.
- [39] M. J. WARD AND J. B. KELLER, *Strong localized perturbations of eigenvalue problems*, SIAM J. Appl. Math., 53 (1993), pp. 770–798.
- [40] H. S. WILEY, S. Y. SHVARTSMAN, AND D. A. LAUFFENBURGER, *Computational modeling of the EGF-receptor system: A paradigm for systems biology*, Trends Cell Biol., 13 (2003), pp. 43–50.
- [41] L. WOLPERT, R. BEDDINGTON, T. JESSEL, P. LAWRENCE, AND E. MEYEROWITZ, *Principles of Development*, Oxford University Press, Oxford, UK, 1998.
- [42] R. ZWANZIG, *Diffusion-controlled ligand-binding to spheres partially covered by receptors - an effective medium treatment*, Proc. Nat. Acad. Sci. U.S.A., 87 (1990), pp. 5856–5857.
- [43] R. ZWANZIG AND A. SZABO, *Time-dependent rate of diffusion-influenced ligand-binding to receptors on cell-surfaces*, Biophys. J., 60 (1991), pp. 671–678.